Please provide feedback

Please support the ScholarWorks@UMBC repository by emailing scholarworks-group@umbc.edu and telling us what having access to this work means to you and why it's important to you. Thank you.

Measuring deadtime and double-counts in a non-paralyzable scintillating neutron detector using arrival time statistics

K. Pritchard [a,b,*], J.P. Chabot [a], P. Tsai [a], R. Robucci [b], F.S. Choa [b], A. Osovizky [c], J. Ziegler [a], E. Binkley [a], N. Hadad [a], M. Jackson [d], C. Hurlbut [d], G.M. Baltic [a], C.F. Majkrzak [a], N.C. Maliszewskyj [a]

[a] *NIST Center for Neutron Research, Gaithersburg, MD, United States of America*
[b] *University of Maryland Baltimore County, MD, United States of America*
[c] *Rotem Industries Ltd, Rotem Industrial Park, Israel*
[d] *Eljen Technology, Sweetwater, TX, United States of America*

ARTICLE INFO

ABSTRACT

A ^{6}LiF:ZnS(Ag) based cold neutron detector with wavelength shifting (WLS) fibers and SiPM photodetector was developed at the NIST Center for Neutron Research for the CANDoR instrument (Chromatic Analysis Neutron Diffractometer or Reflectometer). The scintillation response of ZnS(Ag) to ^{6}Li fission products is a long and irregular delayed fluorescence lasting more than 50 μs. To wait as long as 60 μs for complete fluorescence decay would impose an unreasonably long deadtime to the system and would severely limit the count rate of this detector. A real-time algorithm was implemented to compensate for the long fluorescence decay, reducing but not eliminating sensitivity for a 60 μs period. This greatly reduces the deadtime to approximately 3 μs compared to imposing a 60 μs hold-off time, while also achieving a double-count fraction (counting the same event multiple times) below 1E−4. Timestamping capabilities of the detector system were used to compile arrival time statistics. Comparisons of the measured arrival time statistics with Poisson arrival statistics illustrates features in the fluorescence compensation algorithm and enables the calculation of deadtime and double-count fraction.

1. Introduction

A ^{6}LiF:ZnS(Ag) based cold neutron detector with wavelength shifting (WLS) fibers and SiPM photodetector was developed at the NIST Center for Neutron Research for the CANDoR instrument [1–8]. This detector was developed with the dual purpose of finding a strategic alternative to helium-3, and also because the CANDOR instrument requires an exceptionally thin detector (<2 mm). This paper discusses efforts to minimize the deadtime of this detector and describes a method for gauging the deadtime and double-count fraction (counting the same event multiple times).

Deadtime affects the number of counts observed by a detector system, particularly at high count rates. Fig. 1, illustrates how deadtime effects the measured count rate as a function of the actual count rate for a non-paralyzable detector observing a Poisson process.

The actual count rate of a non-paralyzable detector is calculated from the measured count rate, the detector deadtime, and the background count rate using Eq. (1).

$$n = \frac{m}{1 - m\tau} - b \qquad (1)$$

where n is the actual count rate, m is the measured count rate, τ is the deadtime, and b is the background count rate.

The analytical expressions and models for deadtime are well established by Poisson processes in radiation detection [9–13]. More recent work has been done to model deadtime in non-ideal and non-Poisson situations [14–17].

Deadtime measurements are usually done using one of several methods. The first method is the "two-source" method, whereby count rates are measured in the presence of two constant radiation sources separately, and then together. The combined count rate should be a linear superposition of each source, and any deviation is assumed to be a result of deadtime. The second method is the "fast decaying source" method, where a fast-decaying isotope (a half-life ranging from minutes to hours) is placed in the presence of the detector. For a detector system with a deadtime of zero, the count rate should decay exponentially with the source's radioactivity. Any deviation, particularly during high radioactivity periods, is assumed to be the result of deadtime [9,12, 18]. A third method, called the "pulser" method injects electronically generated pulses into a detection system and observes the deadtime
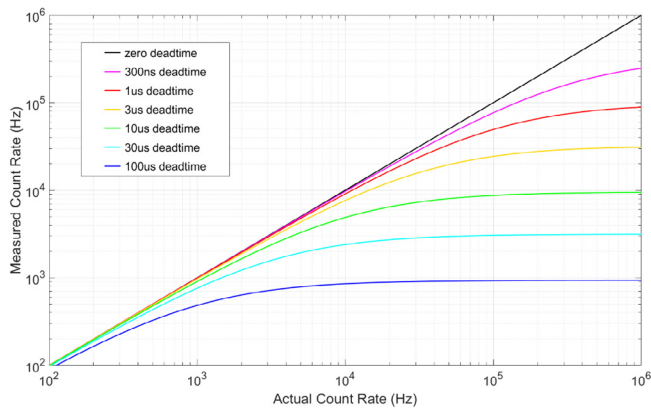
Fig. 1. Deadtime reduces the observed count rate.
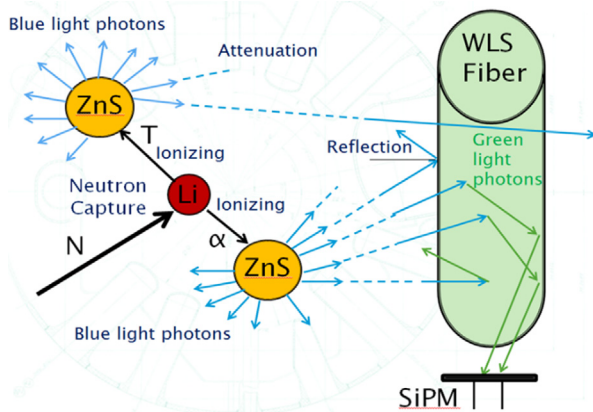
Fig. 2. Diagram of neutron absorption, scintillation, and routing processes.

Fig. 3. Photograph of the detector.

Fig. 4. Photograph of discriminator/timestamper hardware.

effects. The pulser method requires that the electronically generated pulses mimic the size and shape of naturally occurring detector pulses [12,19,20]. A fourth less commonly used method directly analyzes event arrival statistics of a Poisson process [21]. A similar approach is described in this paper, since the "two-source" and "fast decaying source method" methods were not easy to perform in our case. The pulser method was also not feasible because of the variance in size and shape of neutron pulses in the CANDOR detector.

This paper describes a non-paralyzable neutron detector system in the presence of a constant radiation field. The detector/discriminator has event timestamping capability. Neutron events are identified and timestamped using a precision time protocol (PTP) with 100 ns time resolution. After recording a large number of timestamped events, the distribution of arrival times is compared with Poisson arrival statistics in order to determine the system's deadtime.

2. Detector and discriminator description

The CANDOR detector is based on a mixture of ^{6}LiF neutron absorber and ZnS(Ag) scintillator materials. A ^{6}Li nucleus will readily absorb a neutron resulting in a nuclear fission that releases 4.78 MeV of energy in the form of 1 alpha particle and 1 triton particle. The high energy particles ionize ZnS(Ag) scintillator within the mixture, and blue light is emitted via a delayed fluorescence process. The ^{6}LiF:ZnS(Ag) scintillator sheets are sandwiched around a close packed array of wavelength shifting (WLS) fibers. The fibers conduct scintillation light to a silicon photomultiplier (SiPM) photosensor. Fig. 2 shows a diagram of the detector processes. A photograph of the detector is shown in Fig. 3.
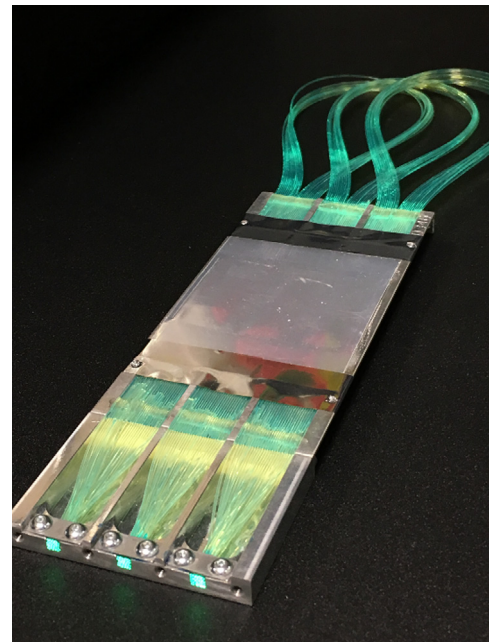
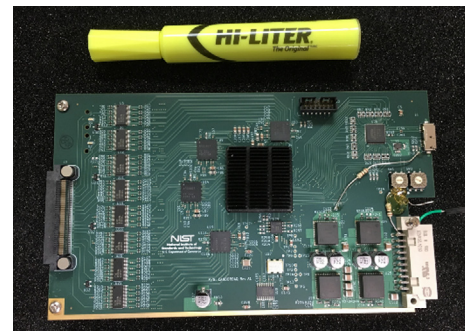The SiPM signal is amplified and sent on to a digitizer PCB named "CANDOR_DAQ" (Fig. 4). This circuit board digitizes the signal at a sampling rate of 50 mega-samples per second (MSPS) using a TI AFE5801 analog-to-digital converter (ADC). The datastream is processed on a Xilinx Kintex-7 field programmable gate array (FPGA), where a pulse shape discrimination algorithm identifies neutrons. If a neutron is detected, the CANDOR_DAQ will generate an event word with a detector address and a PTP timestamp with 100 ns time resolution.

3. Experiment test station

Detectors were tested at the PHADES experiment test station. The PHADES location uses a highly oriented pyrolytic graphite monochromator set at a fixed angle to steer a 4.87 meV (4.1 Å) neutron beam into a shielded cavity formed of borated polyethylene. Post-collimation, the rectangular beam had a width of 5 mm, a height of 20 mm, and the beam current can be varied using borated glass attenuators. A Helium-3 reference detector is placed behind the detector under test. A diagram illustrates the setup in Fig. 5.

4. Long, Irregular Neutron Fluorescence of ^{6}LiF:ZnS(Ag)

Neutron scintillation in ZnS(Ag) is very long lasting. Delayed fluorescence can last up to 60 μs for larger pulses (Fig. 6). The decay
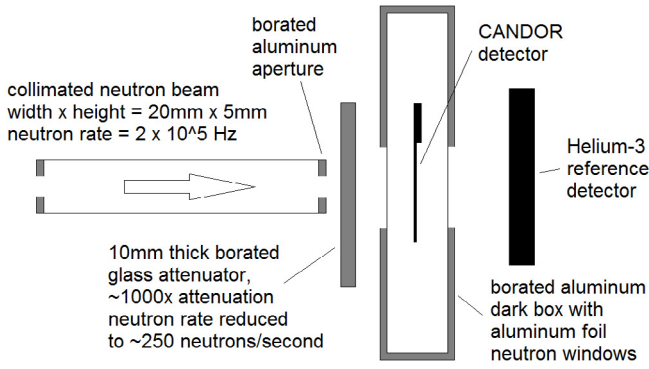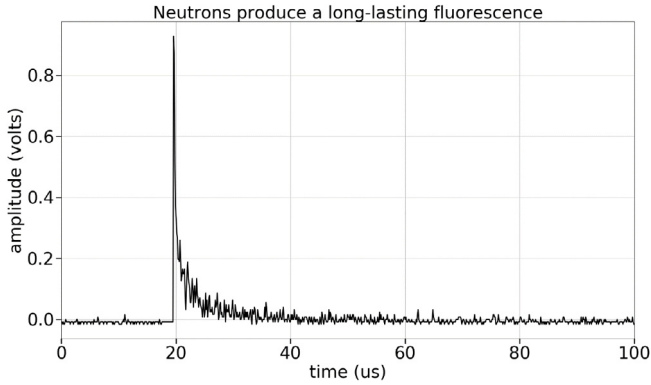
Fig. 5. Detector measurement station diagram.

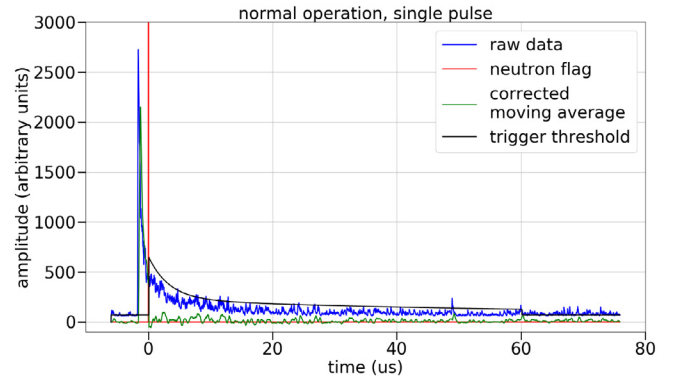Fig. 6. Long fluorescence decay for neutrons.

Fig. 7. Normal operation, single pulse. (For interpretation of the references to color in this figure legend, the reader is referred to the web version of this article.)
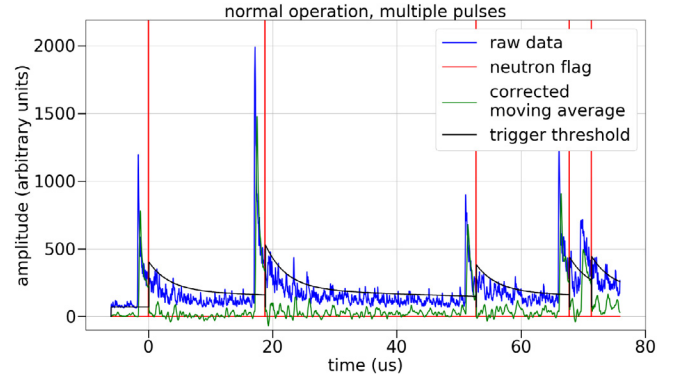

Fig. 8. Normal operation, multiple pulses. (For interpretation of the references to color in this figure legend, the reader is referred to the web version of this article.)

follows an exponential trend, but it is jagged and irregular. A Pulse Shape Discrimination (PSD) algorithm, described elsewhere [2], identifies a neutron within a decision period of 1.4 μs after a rising edge trigger. Since the entire decay of the pulse is dozens of times longer than the PSD decision period, it is possible for the PSD algorithm to "double count" the same pulse after initial identification. To prevent this from happening, either the sensitivity of the discriminator must be eliminated using a long hold-off time, or the fluorescence decay must be compensated for while the sensitivity is reduced.

A hold-off time encompassing the entire 60 μs decay would be far too long, as the count rates would be severely limited. The discriminator must be built in a way to compensate for the fluorescent decay of a preceding pulse while continuing to process new pulses. This is the only way to prevent double-counting while at the same time allowing for a high event processing rate. Since neutron pulses have a large range of magnitudes, the decay compensation also needs to be proportional to the size of the preceding pulse. The act of compensating for the fluorescent decay in a proportional manner will be referred to as "adaptive cooloff". The amount of time the discriminator is insensitive to new events is commonly known as the "deadtime". Lastly, the fraction of neutron events which are counted twice will be referred to as the "double count fraction".

If double-counting cannot be completely eliminated, it must be reduced below a rate of one double-count per 1000 processed pulses or less. A double count fraction of 0.001 (0.1%) is an acceptable measurement error for neutron scattering data. Methods for measuring double count rates will be discussed later along with deadtime analysis. Traditionally, estimating the double-count fraction requires individual inspection of thousands of pulse waveforms. Since individual waveform inspection can be subjective, statistical methods offer a more objective way to assess both the deadtime and the double count fraction of an adaptive cooloff scheme.

The decay shape of our scintillator follows a 2-term exponential decay profile. And, the variance of the signal also has a 2-term exponential decay shape. Our adaptive cooloff algorithm subtracts the expected pulse decay from incoming data, and the trigger threshold for subsequent pulse inspection is raised by a multiple of the signal variance [7].

5. Example waveforms

An internal logic analyzer (ILA) was implanted into the Xilinx Kintex 7 FPGA in order to review the internal workings of the adaptive cooloff algorithm. Figs. 7–10, all show four signals: the raw ADC datastream (blue), the corrected moving average after subtracting the expected fluorescent decay (green), the trigger threshold (black), and a neutron detection flag (red). Fig. 7 shows normal operation. After a neutron detection, the trigger threshold is raised by 5.5 standard deviations of the expected signal variance. The trigger threshold decays exponentially for 60 μs at which point the system returns to normal operation.

Fig. 8 shows the adaptive cooloff at a high count rate, where five neutrons arrive in close succession, and the algorithm successfully identifies all five events.

Fig. 9 shows a smaller pulse arriving during the decay of a larger pulse. The second pulse is too small to re-trigger the discriminator. This is a missed count, and this demonstrates how reduced sensitivity during adaptive cooloff contributes to the deadtime of the detector.

Fig. 10 shows the system double counting a neutron at 35 μs. Note that this waveform is from a separate dataset where the trigger threshold was only raised by 3 standard deviations. There were no double counts observed at the 5.5σ threshold increase.
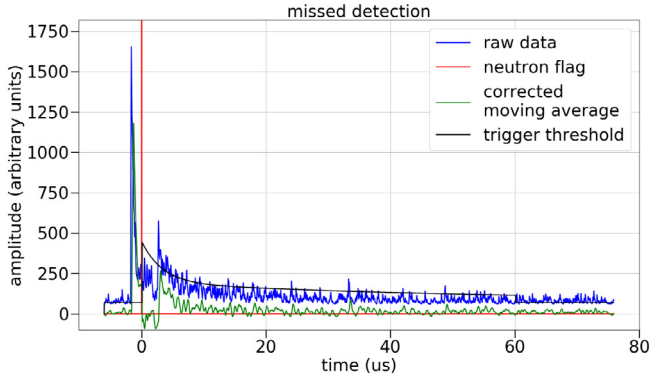
Fig. 9. Missed detection at ~3 us. (For interpretation of the references to color in this figure legend, the reader is referred to the web version of this article.)
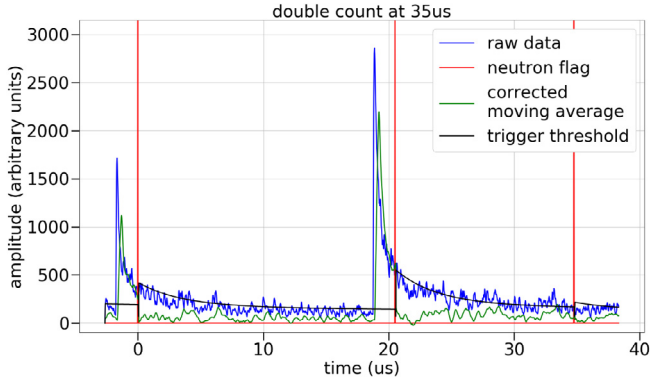

Fig. 10. Double count at 35 us. (For interpretation of the references to color in this figure legend, the reader is referred to the web version of this article.)

Fig. 11. Actual arrival times are compared to the exponential distribution of arrival times for $\lambda = 1562$ s^{-1}.

Fig. 12. Close-up of a measured PDF and exponential distribution.

6. Deadtime calculations based on arrival time statistics

The CANDOR_DAQ has timestamping capability. Each event includes the detector address and the time of arrival with a time resolution of 100 ns, compatible with PTP timing protocols. This allows for a comparison between the measured distribution of arrival times and the exponential distribution of arrival times for a random event. For a random process with an average arrival rate of λ, and the arrivals occur independently, the probability that an event arrives within a particular time period is [10]:

$$P\left(t_1 < X < t_2\right) = e^{-\lambda t_1} - e^{-\lambda t_2} \tag{2}$$

To compute the arrival times of events, and the count rate, a dataset with a very large number of events (>10 million) is gathered by the CANDOR_DAQ. The count rate is measured by dividing the total number of events by the measurement time. The arrival time for each event is calculated by subtracting the previous event timestamp from the current event timestamp. The arrival times are histogrammed, and a probability density function (PDF) is computed by dividing the arrival time histogram by the total number of events. Figs. 11 and 12 show the measured PDF and the exponential distribution for the measured count rate.

There are some features to discuss in the measured PDF of Fig. 12. Beginning at $t = 0$, the probability of detection is zero. This is a firm deadtime for our digital PSD algorithm. After triggering, an event must be integrated for 1.28 μs before the neutron is identified, plus there is a 100 ns period in which the FPGA performs calculations and the adaptive cooloff profile is initialized. At $t = 1.4$ μs, there is a brief spike in sensitivity. This is the first opportunity for the pulse shape
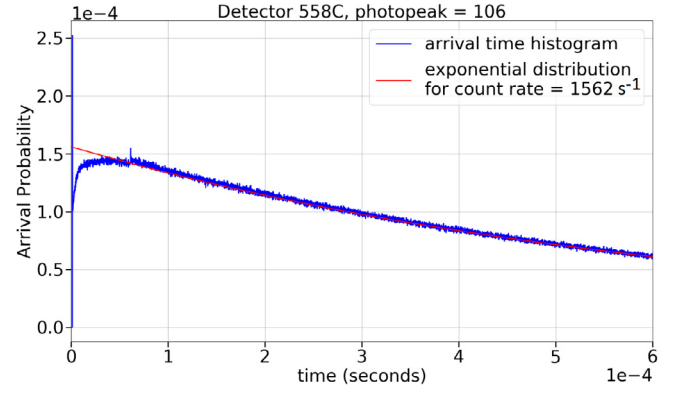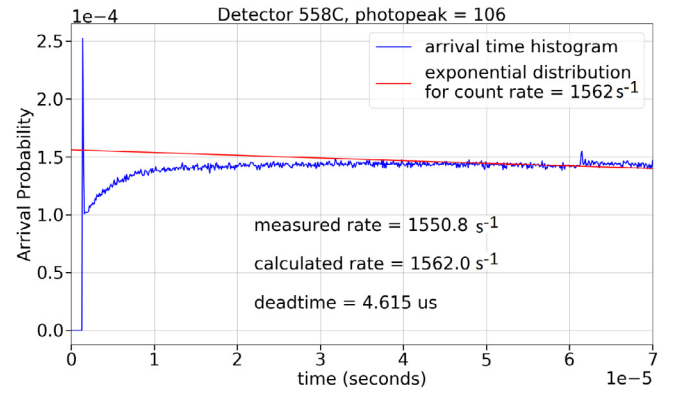
discrimination algorithm to re-trigger. There is a possibility that a second neutron arriving toward the end of the 1.4 μs dead time will be detected once the PSD algorithm resets. After this first opportunity to re-trigger, the sensitivity drops and slowly recovers until the end of the adaptive cooloff period at 61.4 μs. There is also a brief spike in sensitivity just after 61.4 μs when adaptive cooloff ends. If a small neutron pulse arrives near the end of adaptive cooloff, and this event is too small to breach the raised trigger threshold, but large enough to trigger the normal threshold, then it will trigger the PSD algorithm the moment adaptive cooloff ends.

Calculating the deadtime (τ) and the calculated count rate (r) from the measured PDF and the exponential distribution is allowed, given two assumptions. Assumption 1: There is a constant neutron flux flowing into the detector. This assumption appears to be valid for the NCNR reactor source. A spallation neutron source with brief pulses of high neutron intensity is not a Poisson process. Assumption 2: The deadtime is equal to zero after the adaptive cooloff period ends at 61.4 μs. This assumption is logical, because the PSD algorithm has returned to its normal state at this time, and the algorithm is non-paralyzable. Given these assumptions, the deadtime and count rate are calculated by iterating through Eqs. (2)–(5). Deadtime is calculated using Eq. (3).

$$\tau = \sum_{n=0}^{end\ of\ adaptive\ cooloff} \left(1 - \frac{M[n]}{T[n]}\right) \times timestamp\ resolution \tag{3}$$

where $M[n]$ is the measured PDF, $T[n]$ is the theoretical exponential distribution, and n is the timestamp index. The timestamp resolution in our device is 100 ns. After calculating the deadtime, the calculated count rate is found using Eq. (4).

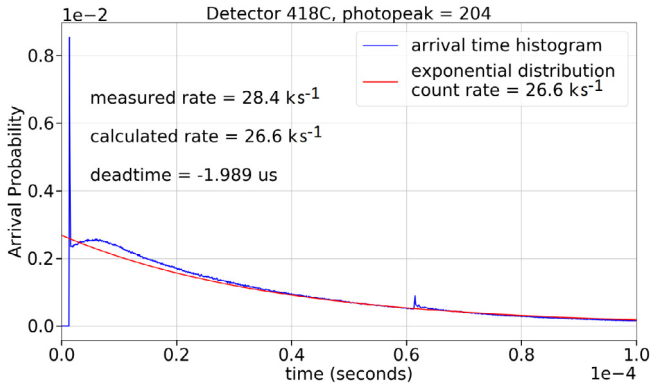$$r_{calculated} = \frac{C_{total}}{T_{total} - C_{total}\tau} \tag{4}$$

Fig. 13. PDF distortion is prevalent at high count rates.

Fig. 14. Deadtime calculations for a progression of count rates. Detector 418C with and adaptive cooloff threshold of 5.5σ (blue), Detector 418C with threshold = 3.25σ (red), Detector 558C with threshold = 5.5σ (green), Detector 558C with threshold = 3.25σ (black).. (For interpretation of the references to color in this figure legend, the reader is referred to the web version of this article.)

where C_{total} is the total number of events in the dataset, and T_{total} is the total collection time. Next, the mean number of arrivals during a timestamp period (λ), is calculated from $r_{calculated}$ and the timestamp resolution.

$$\lambda = r_{calculated} \times timestamp\ resolution \tag{5}$$

The exponential distribution is re-calculated using Eq. (2) and the new value of λ. The whole process involving Eqs. (2)–(5) is iterated 20 times at which point the results converge to their final values.

This measurement procedure is relatively simple for a reactor source with a steady flow of neutrons and a timestamping detector system. This method does not work with a spallation source with brief pulses of high neutron intensity. Also, the measurement must be made using a sufficiently low count rate, and a very large number of events must be observed for adequate statistics.

7. Count rate limitations

A basic property of a probability density function (PDF) is that it integrates to one. Suppressing the sensitivity of a detector during an initial time period causes the PDF to redistribute later in time. This effect is pronounced at high count rates and is observed in Fig. 13. The detection algorithm suppresses the detector's sensitivity to zero during the 0 µs to 1.4 µs evaluation period following a rising edge trigger. A second neutron cannot be detected during this initial 1.4 µs period. As a result, the PDF redistributes, and the detection probability is elevated at other times. In Fig. 13, this is observed in the local maximum of the arrival time histogram at $t = 6$ µs, exceeding the exponential distribution. The elevated probability of arrival during the deadtime calculation period (0 µs–62.4 µs) exceeds the exponential distribution for a Poisson process, resulting in a negative deadtime calculation at very high count rates.

PDF distortion during the deadtime calculation period is insignificant at low count rates. PDF distortion after the deadtime calculation period, although necessarily present, does not affect the deadtime calculation (Eq. (3)). An appropriate range of count rates was found empirically by performing deadtime measurements at a progression of count rates (Fig. 14). In Fig. 14, count rates above 1 ks^{-1} accompany enough PDF distortion to artificially lower the deadtime calculation. Therefore, only count rates below 1 ks^{-1} are considered to yield valid deadtime calculations for our detector system.

In Fig. 14, two different detectors were tested, detector 418C and detector 558C. These two detectors have different optical quality. Detector 418C has superior optical quality, whereas detector 558C yields fewer photons and smaller pulses in response to neutron absorption. Most pulses generated in detector 418C are larger, easier to discriminate, and these larger pulses arriving during the adaptive cooloff period are much more likely to be counted. This means that we
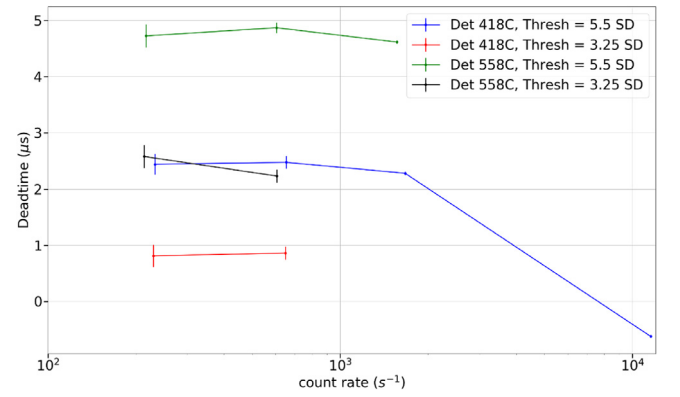
expect detector 418C to have a shorter deadtime than detector 518C. We also tested two different adaptive cooloff thresholds, 5.5 σ and 3.25 σ. We expected that the higher adaptive cooloff threshold would have a longer deadtime.

Fig. 14 shows convergence of the deadtime calculations below a count rate of 700 s^{-1}. This convergence shows that an appropriate count rate has been achieved below 700 s^{-1}, and that PDF distortion is acceptably low.

Detector 418C with a 3.25σ threshold has a very low deadtime, between 800 ns and 900 ns. This seems almost impossibly low, given that there is a fixed deadtime of 1.4 µs dictated by the integration time and processing time of the pulse shape discriminator. However, many pulses can be detected hundreds of nanoseconds after their rising edge as shown by the sensitivity spike at 1.4 µs in Figs. 12 and 13. The PDF of this detector configuration does not look abnormal, and it could be that the deadtime is indeed that low. There is also the possibility that some pulses are double-counted to give an erroneous deadtime measurement, and this possibility is explored next.

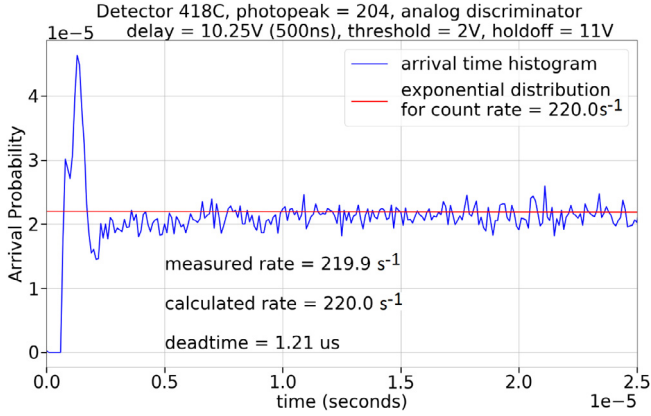## 8. Arrival time PDF for an analog discriminator

The arrival time PDF and deadtime were examined for a separate pulse shape discriminator composed of discrete components (amplifiers, integrating circuits, comparators, etc.). This "analog discriminator" outputs a logic pulse upon identifying a neutron, and this logic pulse was input into the CANDOR_DAQ for timestamping. The internal workings of this discriminator are described elsewhere [7]. The analog discriminator is an effective alternative to the digital system described earlier. The arrival time statistics of this analog discriminator also offer some interesting insights (Figs. 15 and 16).

Looking at the statistics for the analog discriminator, there is a brief period of complete deadtime ($t = 0$ ns thru $t = 500$ ns) followed by a period where double counts are prevalent ($t = 500$ ns thru $t = 1.5$ µs), and then a longer period where there is reduced sensitivity which eventually recovers to baseline before 20 µs. This is an interesting case, because this PDF contains a mixture of double-counts as well as missed counts. How many double-counts are in this mixture? How many missed counts? These questions cannot be answered from a single PDF.

Fig. 16 shows a second arrival time PDF for the same detector configuration. Only the count rate has increased. The count rate was increased from 220.0 s^{-1} to 631.5 s^{-1} resulting in changes to the double-count and deadtime features. At higher count rates, the number of missed counts dominates, but at low count rates there is a higher proportion of double counts. This is logical after considering that the

Table 1
Results of deadtime and double-count fraction measurements.

Detector	Adaptive cooloff threshold	Deadtime	1σ deadtime uncertainty	Double-count fraction	1σ double-count uncertainty
418C	Analog	2.42 µs	0.15 µs	2.68E−04	1.09E−04
558C	Analog	6.47 µs	0.15 µs	1.07E−03	8.23E−05
418C	5.5σ	2.49 µs	0.14 µs	9.85E−06	1.06E−04
558C	5.5σ	4.90 µs	0.13 µs	4.13E−05	8.78E−05
418C	3.25σ	0.90 µs	0.15 µs	1.95E−05	1.08E−04
558C	3.25σ	2.04 µs	0.14 µs	−1.13E−04	1.00E−04

Fig. 15. Arrival time PDF and exponential distribution for analog discriminator, 220.0 s^{-1}.
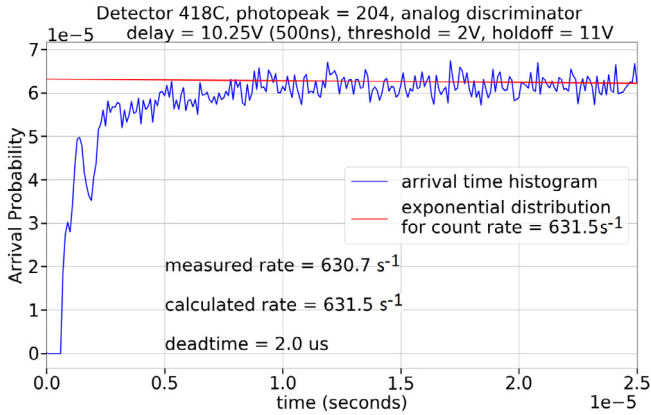
Fig. 16. Arrival time PDF and exponential distribution for analog discriminator, 631.5 s^{-1}.

deadtime fraction increases linearly with the count rate, but the double-count fraction should remain constant regardless of count rate. The double count fraction, in theory, is not a function of how frequently events arrive, but rather a function of the variability in decay shapes and the adaptive cooloff threshold. *Double-count fraction constancy* and *linear increase of deadtime fraction* with count rate can be exploited to determine both the double-count fraction and the deadtime.

9. Determining deadtime and double-count fraction from arrival time PDFs

A solvable system of equations can be derived from Eq. (6):

$$measured\ counts = theoretical\ counts - missed\ counts + double counts \quad (6)$$

where theoretical counts follow the exponential distribution of arrival times for a given count rate. The number of missed counts is expressed as:

$$missed\ counts = theoretical\ counts \times \tau \times r_c \quad (7)$$

where τ is the deadtime and r_c is the calculated count rate. The number of missed counts is equal to the theoretical number of counts multiplied by the deadtime fraction. The number of double counts is:

$$double\ counts = theoretical\ counts \times d \quad (8)$$

where d is the double-count fraction. Eqs. (6)–(8) are consolidated into Eq. (9):

$$M = T(1 - \tau r_c + d) \quad (9)$$

where M is the number of measured counts and T is the number of theoretical counts. If measurements are taken at two different count rates, a system of two equations can be generated.

$$\begin{aligned} M_1 &= T_1(1 - \tau r_1 + d) \\ M_2 &= T_2(1 - \tau r_2 + d) \end{aligned} \quad (10)$$

The deadtime (τ) and double-count fraction (d) are assumed to be constant for both measurements. We now have two equations and two unknowns which can be solved.

$$\tau = \frac{\frac{M_2}{T_2} - \frac{M_1}{T_1}}{r_1 - r_2}$$
$$d = \frac{M_1}{T_1} + \tau r_1 - 1 \quad (11)$$

Since it is the M/T ratio that is important, we can set T equal to 1, and M is computed as:

$$M = 1 - \left(\sum_{n=0}^{end\ of\ adaptive\ cooloff} T[n] - M[n] \right) \quad (12)$$

where $M[n]$ is the measured PDF, $T[n]$ is the exponential distribution, and n is the timestamp number. The deadtime and double-count fraction were determined for six detector configurations and tabulated in Table 1. Each configuration was tested at two different count rates approximately 230 s^{-1} and 600 s^{-1}. Deadtime and double-count fraction were computed using Eqs. (11) and (12). These count rates were found previously to have acceptably low PDF distortion during the deadtime calculation period.

The six test cases include two different detectors: 418C and 558C. Detector 418C was described earlier as having superior optical quality. The six test cases also encompass three different discriminator configurations: the CANDOR_DAQ digital discriminator with two adaptive cooloff thresholds of 3.25σ and 5.5σ, and the analog discriminator at a single configuration.

The values and uncertainties in Table 1 result from approximately 1E+7 events per PDF measured over a period of many hours. Each row in the table required two PDFs measured at two different rates. Each row reflects a full day of beamtime at PHADES to gather a 6-hour exposure at ~600 s^{-1} and an 18-hour exposure at ~250 s^{-1}.

10. Conclusion & future work

The deadtime measurements and calculations described in this paper are a different approach to the well established *two-source method* and *fast-decaying source* method. Unfortunately, these established methods were not used to corroborate this *arrival statistics method*. Even so, the results of the *arrival statistics method* appear reasonable, and the

calculated numbers seem to reflect the trends seen in the arrival time PDF as well as our expectations.

The arrival time PDFs enable some unique advantages. Previously, there was no statistical way to determine the double-count fraction other than the very tedious, subjective, and sometimes unreliable practice of manually inspecting waveforms. Arrival time PDFs also allow a designer to view where in time the adaptive cooloff profile might be too lenient allowing double counts, or too strict with very low sensitivity. This could inform optimizations for the adaptive cooloff profile's shape and duration. Additionally, the *arrival time method* for measuring deadtime is a relatively simple measurement procedure and can be done in-situ.

11. Disclaimer

Certain commercial equipment, instruments, or materials (or suppliers, or software, . . .) are identified in this paper to foster understanding. Such identification does not imply recommendation or endorsement by the National Institute of Standards and Technology, nor does it imply that the materials or equipment identified are necessarily the best available for the purpose.

CRediT authorship contribution statement

K. Pritchard: Methodology, Formal analysis, Investigation, Writing. **J.P. Chabot:** Resources. **P. Tsai:** Resources. **R. Robucci:** Supervision. **F.S. Choa:** Supervision. **A. Osovizky:** Supervision. **J. Ziegler:** Resources. **E. Binkley:** Resources. **N. Hadad:** Project administration. **M. Jackson:** Resources. **C. Hurlbut:** Resources. **G.M. Baltic:** Funding acquisition. **C.F. Majkrzak:** Supervision, Conceptualization. **N.C. Maliszewskyj:** Supervision, Conceptualization.

Declaration of competing interest

The authors declare the following financial interests/personal relationships which may be considered as potential competing interests: The CANDOR project received funding from the Center for High Resolution Neutron Scattering (CHRNS). CHRNS is a national user facility jointly funded by the NIST Center for Neutron Research (NCNR) and the National Science Foundation (NSF) under Agreement No. DMR-2010792.

References

[1] CHRNS CANDOR - White-Beam Reflectometer, 2020, https://www.nist.gov/ncnr/chrns-candor-white-beam-reflectometer.

[2] K. Pritchard and, et al., 6LiF:ZnS(Ag) neutron detector performance optimized using waveform recordings and ROC curves, IEEE Trans. Nucl. Sci. 67 (1) (2020) 414–421.

[3] N.C. Maliszewskyj, et al., An energy analyzing detector for cold neutrons, 2018.

[4] A. Osovizky, et al., 6LiF:ZnS(Ag) mixture optimization for a highly efficient ultrathin cold neutron detector, 2018.

[5] A. Osovizky, et al., Design of an ultrathin cold neutron detector, 2018.

[6] A. Osovizky, et al., Selection of silicon photomultipliers for a 6LiF:ZnS(Ag) scintillator based cold neutron detector, J. Phys. Commun. 2 (4) (2018) 045009, http://dx.doi.org/10.1088/2399-6528/aab381.

[7] K. Pritchard, Signal Processing, Performance Metrics, and Lifetime of a 6LiF:ZnS(Ag) Neutron Detector with WLS Fibers and SIPM Photodetector (Dissertation), University of Maryland Baltimore County, 2020.

[8] K. Pritchard and, et al., Cold neutron radiation dose effects on a 6LiF:ZnS(Ag) neutron detector with wavelength shifting fibers and SiPM photodetector, TBA.

[9] G. Knoll, Radiation Detection and Measurement, fourth ed., John Wiley & Sons, Inc., United States, 2010.

[10] Jorg Muller, Counting Statistics of a Poisson Process with Deadime, Report BIPM-111, 1970.

[11] Jorg Muller, On the interval-distributions for recurrent events with a non-extended dead time, in: BIPM-105, 1967.

[12] S. Usman, A. Patil, Radiation detector deadtime and pile up: A review of the status of science, Nucl. Eng. Technol. 50 (7) (2018) 1006–1016, http://dx.doi.org/10.1016/j.net.2018.06.014.

[13] L. Takacs, On probability problems in the theory of counters, Ann. Math. Stat. 29 (4) (1958) 1257–1263.

[14] B. Denecke, S. de Jonge, An analyzer for pulse-interval times to study high-order effects in the processing of nuclear detector signals, Appl. Dadiat. Isot. 49 (9–11) (1998) 1099–1105.

[15] V. Bécares, J. Blázquez, Detector dead time determination and optimal counting rate for a detector near a spallation source or a subcritical multiplying system, Sci. Technol. Nucl. Install. 2012 (2012) 1–7, http://dx.doi.org/10.1155/2012/240693.

[16] S.H. Lee, R.P. Gardner, M. Jab, Determination of Dead Times in the Recently Introduced Hybrid G-M Counter Dead Time Model, 2004, p. 5.

[17] V. Kornilov, Effects of dead time and after-pulses in photon detector on measured statistics of stochastic radiation, J. Opt. Soc. Amer. A 31 (1) (2014) 7, http://dx.doi.org/10.1364/JOSAA.31.000007.

[18] A. Patil, Dead time and count loss determination for radiation detection systems in high count rate applications, p. 79.

[19] M.G. Strauss, L.L. Sifter, F.R. Lenkszus, R. Brenner, Ultra stable reference pulser for high resolution spectrometers, IEEE Trans. Nucl. Sci. 15 (3) (1968) 518–530, http://dx.doi.org/10.1109/TNS.1968.4324977.

[20] F.L.R. Vinagre, C.A.N. Conde, Method for effective dead time measurement in counting systems, Nucl. Instrum. Methods Phys. Res. A 462 (3) (2001) 555–560, http://dx.doi.org/10.1016/S0168-9002(01)00179-6.

[21] M. Arkani, G. Raisali, Measurement of dead time by time interval distribution method, Nucl. Instrum. Methods Phys. Res. A 774 (2015) 151–158, http://dx.doi.org/10.1016/j.nima.2014.11.069.